

Highlights

K-Space-Aware Cross-Modality Score for Quality Assessment of Synthesized Neuroimages

Guoyang Xie, Jinbao Wang, Yawen Huang, Jiayi Lyu, Feng Zheng, Yefeng Zheng, Yaochu Jin

- We propose a new metric, called K-CROSS, to evaluate the quality of the synthetic data based on all the structural information, k-space feature shift, and lesion area. This multidimensional quantification indication enables K-CROSS to achieve more precise results than other metrics that only consider natural images.
- To properly verify the effectiveness of our K-CROSS, we construct a large-scale and multi-modal neuroimaging perceptual similarity (NIRPS) dataset, which includes 6,000 assessments from radiologists.
- K-CROSS achieves highly competitive results based on the judgments from radiologists on NIRPS, which can be treated as a general evaluation metric for various purposes of medical image synthesis.

K-Space-Aware Cross-Modality Score for Quality Assessment of Synthesized Neuroimages

Guoyang Xie^{a,b,*}, Jinbao Wang^{c,*}, Yawen Huang^{d,*}, Jiayi Lyu^e, Feng Zheng^{a,**}, Yefeng Zheng^d and Yaochu Jin^f

^aSouthern University of Science and Technology, Department of Computer Science, Shenzhen, 518055, China

^bCATL, Department of Intelligent Manufacturing, Ningde, 352000, China

^cShenzhen University, National Engineering Laboratory for Big Data System Computing Technology, Shenzhen, 518060, China

^dTencent YouTu Lab, Jarvis Research Center, Shenzhen, 510310, China

^eUniversity of Chinese Academy of Sciences, the School of Engineering Science, Beijing, 100049, China

^fWestlake University, the School of Engineering, Hangzhou, 310030, China

ARTICLE INFO

Keywords:

Medical image

Image quality assessment

Cross-modality neuroimage synthesis

K-space

ABSTRACT

The problem of how to assess cross-modality medical image synthesis has been largely unexplored. The most used measures like PSNR and SSIM focus on analyzing the structural features but neglect the crucial lesion location and fundamental k-space speciality of medical images. To overcome this problem, we propose a new metric K-CROSS to spur progress on this challenging problem. Specifically, K-CROSS uses a pre-trained multi-modality segmentation network to predict the lesion location, together with a tumor encoder for representing features, such as texture details and brightness intensities. To further reflect the frequency-specific information from the magnetic resonance imaging principles, both k-space features and vision features are obtained and employed in our comprehensive encoders with a frequency reconstruction penalty. The structure-shared encoders are designed and constrained with a similarity loss to capture the intrinsic common structural information for both modalities. As a consequence, the features learned from lesion regions, k-space, and anatomical structures are all captured, which serve as our quality evaluators. We evaluate the performance by constructing a large-scale cross-modality neuroimaging perceptual similarity (NIRPS) dataset with 6,000 radiologist judgments. Extensive experiments demonstrate that the proposed method outperforms other metrics, especially in comparison with the radiologists on NIRPS. To foster reproducibility and accessibility, the source code is uploaded to the website: <https://github.com/M-3LAB/K-CROSS>

1. Introduction

PSNR (Huynh-Thu and Ghanbari, 2008), SSIM (Wang, Bovik, Sheikh and Simoncelli, 2004), and MAE (Chai and Draxler, 2014) are the most commonly used evaluation metrics in cross-modality magnetic resonance imaging (MRI) synthesis works. However, these metrics are inappropriate to a certain degree, considering that they are based on natural images and naturally ignore the inherent properties of MRI data. In general, the quality of neuroimage can be assessed by the content (*i.e.*, lesion region), frequency space, and structure details. Although MAE, PSNR and SSIM are effective in assessing image quality, they are ineffective as a neuroimage metric, because they only focus on the structural details in the pixel space. Therefore, it is important to find a new way to measure how good the cross-modality neuroimage synthesis is. To foster reproducibility and accessibility, the source code is uploaded to .

Empirically, the content details of neuroimages, particularly the texture and brightness, are disregarded by either PSNR or SSIM. Instead, radiologists pay more attention to the lesion regions, since the usefulness of analyzing pathology and human cognitive functions. The purpose of K-CROSS is to fully reflect the lesion region by introducing a cross-modality neuroimage segmentation network which has already been trained to precisely forecast the tumor location. The prediction mask (*i.e.*, tumor region) is fed into the proposed tumor encoder to extract features. The proposed tumor loss function improves the extracted feature to capture more essential texture details and brightness

*Contributed Equally

**Corresponding Author

✉ guoyang.xie@ieee.org (G. Xie); wangjb@szu.edu.cn (J. Wang); bear_huang@126.com (Y. Huang);

lyujiayi21@mails.ucas.ac.cn (J. Lyu); f.zheng@ieee.org (F. Zheng); yefengzheng@tencent.com (Y. Zheng);

jinyaochu@westlake.edu.cn (Y. Jin)

ORCID(s):

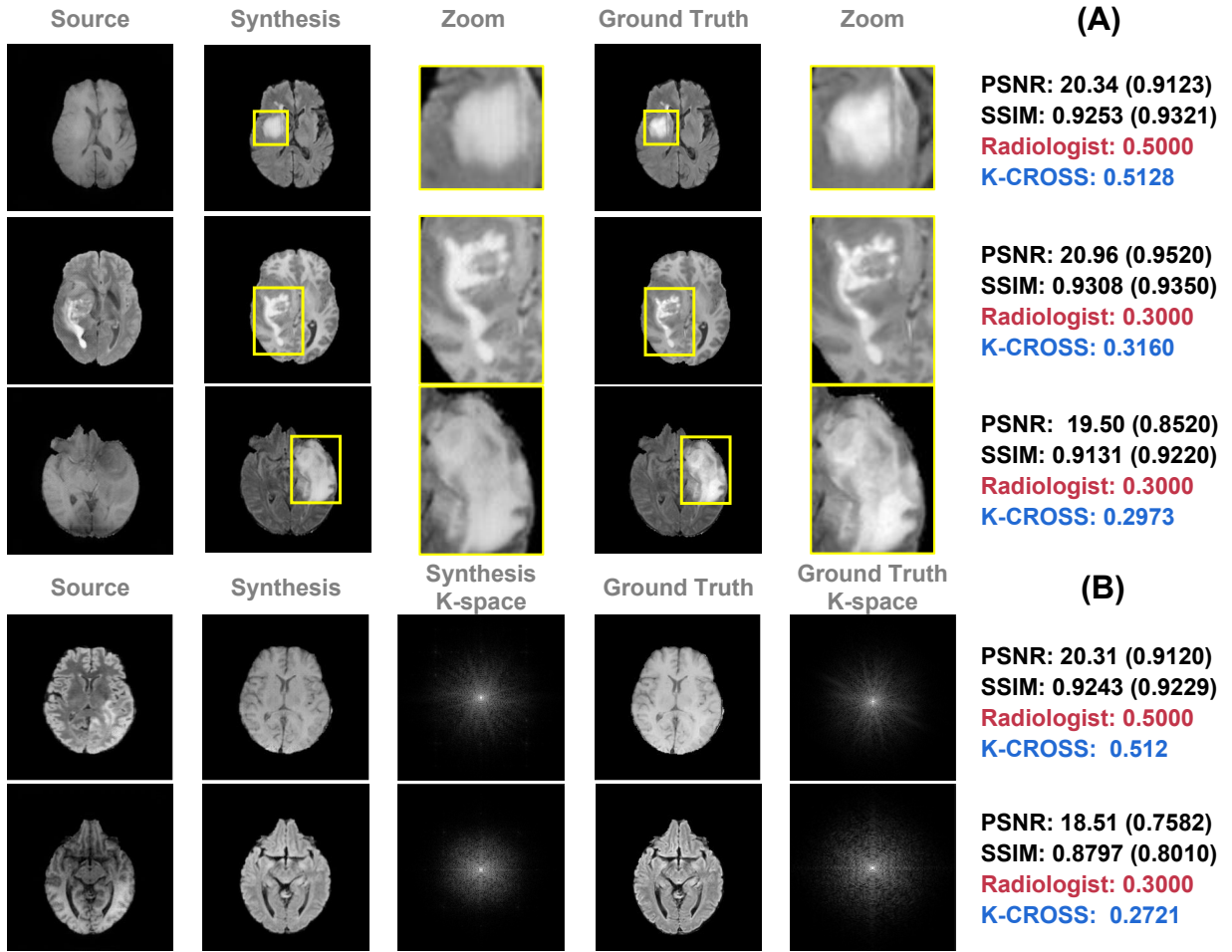


Figure 1: K-CROSS vs. PSNR vs. SSIM. The first and second columns on the left represent the source and synthesized target modality data, respectively. The zoom indicates the modality-specific tumor region, which is provided by the pre-trained multi-modality neuroimage segmentation network. The numbers on the right represent PSNR, SSIM, radiologist score, and our K-CROSS value. PSNR, SSIM, and K-CROSS are rescaled (to 1.0000) for comparison with the radiologist's score. In terms of lesion region and k-space measurement, K-CROSS is more compatible with the radiologist's score than PSNR and SSIM.

information. In Fig. 1 (A), we can observe that the content of the synthesis neuroimage does not align with the target modality neuroimage. Though PSNR and SSIM scores are the highest for the synthesized ones, they only evaluate the structure details without taking the content into account. By contrast, K-CROSS is reliable in exploring neuroimaging perceptual similarity (NIRPS) for the synthesized results.

Besides, PSNR and SSIM are unable to account for differences in the k-space between the synthesized images and the target modality data, whereas K-CROSS can. The fundamental difference between MRI and natural images, as seen from the standpoint of imaging principles, is the basis of MR image reconstruction. The Fourier transformation, often known as the "k-space" in MRI, is a mathematical concept that calculates various frequencies mixed into the received signal of all spins. It forms the basis for all image reconstruction in MRI. Therefore, we believe that the proposed metric can estimate the distance between MRIs in both k-space and pixel space. In k-space, the sophisticated K-CROSS encoder can capture the invariant modal-specific feature, where the frequency loss can be used to further enhance the complicated encoder. When a k-space shift occurs, as seen at the bottom of Fig. 1 (B), K-CROSS is more stable in accordance with the radiologist's score, which is able to measure the gap in k-space between the synthesized neuroimage and the corresponding ground truth.

To constrain the structural features that are extracted by the shared structure encoder from both the source modality and the target modality, we set up a cross-modality similarity loss function, as the entire structure information between the source and the target modality neuroimaging data is very similar. PSNR and SSIM, on the other hand, only assess the input image, which limits their capacity to recognize the structural details that the source modality and the target modality share.

Our contributions can be summarized as follows:

- We propose a new metric, called K-CROSS, to evaluate the quality of the synthetic data based on all the structural information, k-space feature shift, and lesion area. This multidimensional quantification indication enables K-CROSS to achieve more precise results than other metrics that only consider natural images.
- To properly verify the effectiveness of our K-CROSS, we construct a large-scale and multi-modal neuroimaging perceptual similarity (NIRPS) dataset, which includes 6,000 assessments from radiologists.
- K-CROSS achieves highly competitive results based on the judgments from radiologists on NIRPS, which can be treated as a general evaluation metric for various purposes of medical image synthesis.

The rest of this paper is organized as follows: Section 2 presents a literature review on image quality assessment and GAN-based assessment methods. Section 3 explains the proposed algorithm K-CROSS in detail. In addition, a large-scale multi-modal neuroimaging perceptual similarity (NIRPS) dataset is constructed in Section 4. Section 5 presents comprehensive experimental evaluations while Section V draws the conclusion and limitation of the current work.

2. Related Work

2.1. Image Quality Assessment

Image quality assessment (IQA) can be divided into two categories. One is fully referenced IQA, and the other is non-referenced IQA (Mittal, Soundararajan and Bovik, 2013; Moorthy and Bovik, 2011; Bosse, Maniry, Wiegand and Samek, 2016; Talebi and Milanfar, 2018). IQA with all references refers to estimating the quality of natural images with references: SSIM (Wang et al., 2004), MS-SSIM (Wang, Simoncelli and Bovik, 2003) and FSIM (Zhang, Zhang, Mou and Zhang, 2011), focus more on image structure specifics. Specifically, FSIM builds up a novel feature similarity index according to the phase congruence and image gradient magnitude, while PSNR focuses on edge estimation for the synthesized images. Most of them (Lin and Wang, 2018; Ren, Chen and Wang, 2018; taek Lim, Kim and Ro, 2018; Zhang, Ma, Zhai and Yang, 2021) use low-level features for evaluation. LPIPS (Zhang, Isola, Efros, Shechtman and Wang, 2018) is the first work that uses a high-level feature for fully referenced IQA in light of the popularity of deep learning. Estimating the synthesized image quality without a reference (ground truth) is known as non-referenced IQA (Mittal et al., 2013; Moorthy and Bovik, 2011; Bosse et al., 2016; Talebi and Milanfar, 2018). RankIQA (Liu, van de Weijer and Bagdanov, 2017b) is the mainstream for non-referenced IQA. Considering the limited size of IQA, Liu *et al.* propose a Siamese network to rank images and their distorted ones. The Siamese network's knowledge (ranking result) can be transferred to a conventional neural network, whose function is to assess the quality of a single image. Since K-CROSS requires a reference image for evaluation, it belongs to a fully referenced IQA. However, few public data in the medical imaging community could be used to train for the learning-based fully referenced IQA methods. The NIRPS dataset, the first extensive neuroimaging perceptual similarity dataset with radiologists' labels is constructed. As for fully referenced IQA methods, K-CROSS is, therefore, able to use the supervised training methods.

2.2. GAN Assessment

The existing sample-based methods (Xu, Huang, Yuan, Guo, Sun, Wu and Weinberger, 2018) have been proposed to access GAN performance, like Kernel MMD (Gretton, Sriperumbudur, Sejdinovic, Strathmann, Balakrishnan, Pontil and Fukumizu, 2012), Inception Score (Salimans, Goodfellow, Zaremba, Cheung, Radford and Chen, 2016), Mode Score (Che, Li, Jacob, Bengio and Li, 2017) and FID (Heusel, Ramsauer, Unterthiner, Nessler and Hochreiter, 2017). The classical approach is to compare the log-likelihood of generative models. But this approach cannot accurately indicate the quality of synthesized image. In other words, a model can achieve high likelihood, but low image quality, and conversely, low image quality, and conversely. As for Inception score (Salimans et al., 2016), it computes the KL divergence between the conditional class distribution and the marginal class distribution over the generated data. However, IS does not capture intra-class diversity, which is insensitive to the prior distribution over labels. Among

them, the most popular metric is FID. Heusel *et al.* (Heusel et al., 2017) use InceptionV3 (Szegedy, Vanhoucke, Ioffe, Shlens and Wojna, 2016) to extract the features from the real and synthetic neuroimaging data, and then compute the differences in the features between them. However, the majority of them are created in the pixel space and ignore the lesion region and k-space, which are the fundamental elements of MR image properties. In this regard, K-CROSS considers the underlying MR imaging principle as well as the difference between the neuroimages of the source and target modality.

2.3. Cross-Modality Medical Image Synthesis

Existing medical image-to-image translation (Jiang, Lu, Wei and Xu, 2019; Ren, Dey, Fishbaugh and Gerig, 2021; Kong, Lian, Huang, Li, Hu and Zhou, 2021) has demonstrated their considerable research and clinical analysis potential. Of these methods, supervised GANs are still the mainstream for cross-modality neuroimaging data synthesis (Wang, Zhou, Wang, Yu, Zu, Lalush, Lin, Wu, Zhou and Shen, 2018; Dar, Yurt, Karacan, Erdem, Erdem and Çukur, 2019; Sharma and Hamarneh, 2020; Yu, Zhou, Wang, Shi, Fripp and Bourgeat, 2020; Yu, Zhou, Wang, Fripp and Bourgeat, 2018; Zuo, Zhang and Yang, 2021). For instance, Elad *et al.* (Elad, 2012) provide a concise overview of sparse and redundant representation modeling and identify ten important future research directions for sparse coding. Rubinstein *et al.* (Rubinstein, Bruckstein and Elad, 2010) explicate the dictionary acquisition process through mathematical models. Gao *et al.* (Gao, Tsang and Chia, 2012) develop a hypergraph Laplacian matrix to retain the local information of the training samples, thereby enhancing the discriminative capacity of the learned dictionary. However, synthesizing in a supervised manner requires paired data for training, which is difficult to implement in practice. To solve this problem, both semi-supervised and unsupervised methods are then launched to eliminate the need of paired data. (Guo, Wang, Yasarla, Zhou, Patel and Jiang, 2021) leverage a lesion segmentation network as a teacher to guide the generator by using unpaired training data. (Shen, Zhu, Wang, Xing, Pauly, Turkbey, Harmon, Sanford, Mehralivand, Choyke, Wood and Xu, 2021) and (Zhou, Liu and Duncan, 2021) also utilize the high-level tasks to guide the cross-modality image synthesis. Huang *et al.* (Huang, Zheng, Wang, Jiang, Wang and Shao, 2020b; Huang, Zheng, Cong, Huang, Scott and Shao, 2020a) make full use of unpaired cross-modality data and project them into a common space. The attributed features from the common space bring great helpful to synthesize the missing target modality data. (Li, Wu, Wang, Mao, Alsaadi and Zeng, 2022) employ the dual-domain attention mechanism to extract highly discriminative features on the lesion area. Yu *et al.* (Yu, Zhai, Han, Peng and Zhang, 2021) present a similar work with the method shown in (Huang et al., 2020a). However, the authors pay more attention to the mouse brain dataset. Chen *et al.* (Chen, Dou, Chen, Qin and Heng, 2020) propose a more concise idea, i.e., the source modality and the target modality share their feature encoder. Jiao *et al.* (Jiao, Namburete, Papageorghiou and Noble, 2020) also extract and map features into the common space using different modalities. Moreover, the authors in (Jiao et al., 2020) design a new cross-modal attention module for fusion and propagation. Zeng *et al.* (Zeng and Zheng, 2019) use two models; one of which is the 3D generator network, and the other is the 2D discriminator. The authors utilize the result from the 2D discriminator treated as a weak label to supervise the 3D generator, such that the generator's output can be closer to the output of CT. Yang *et al.* (Yang, Sun, Yang and Xu, 2021) design a unified generator for MRI synthesis. (Wu, Wang, Zheng, Li, Alsaadi and Zeng, 2023) propose a MRI oriented novel attention-based glioma grading network into multi-scale feature extraction process, which aims to promote the synergistic interaction among different modality information. (Kong et al., 2021) introduce a new I2IT model called RegGAN, which converts the unsupervised I2IT task into a supervised I2IT with noisy labels. K-CROSS serves as a general metrics for various levels of supervision of cross-modality medical image synthesis.

3. Proposed Method

3.1. Preliminary

3.1.1. K-Space Representations

The spatial frequencies of an MR picture are represented in k-space by a matrix of numbers. Despite MR images and k-space having the identical dimension, in practice, each point (k_x, k_y) in k-space represents the spatial frequency and phase information about each pixel in the MR image rather than corresponding to a specific pixel value. By contrast, every pixel in the MR image maps to a point in k-space. As a result, we transform MRI into k-space using the 2D

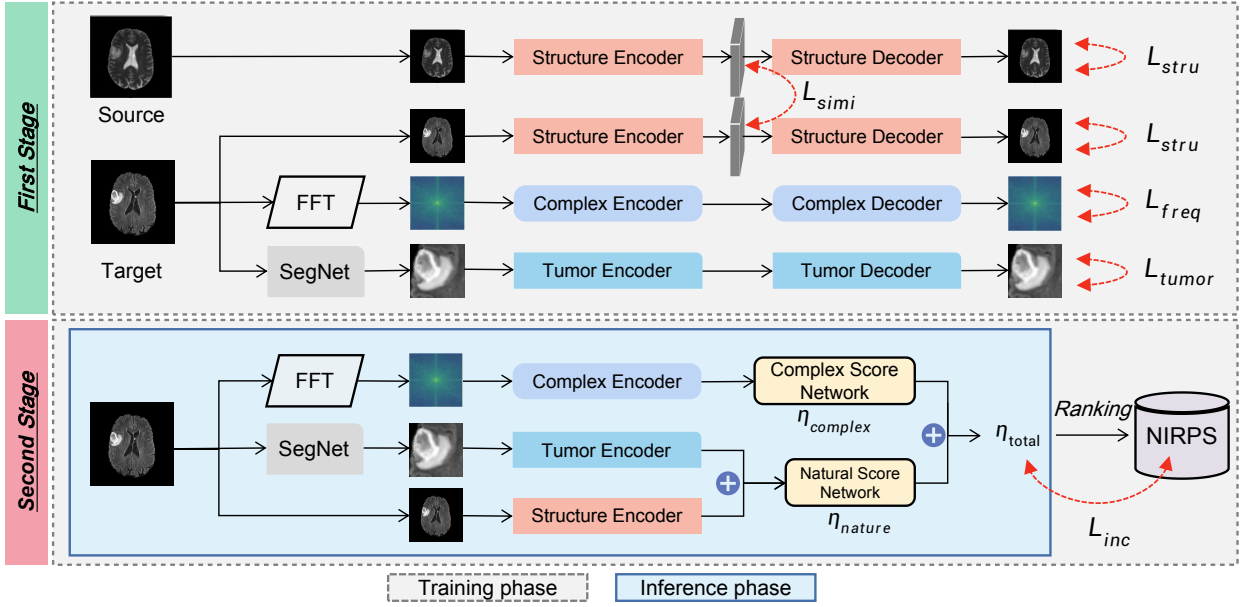


Figure 2: Flowchart of our proposed K-CROSS. **First stage input:** For reference neuroimage (source modality) and its query neuroimage (the target modality), the private portion is indicated by a blue box. The neuroimage's structural feature is captured by the structure encoder. The reconstruction specifics are evaluated using L_{stru} . With a similarity loss L_{simi} , the presentation of the shared structure is maintained. The k-space feature to a modality is captured by Complex U-Net and optimized by L_{freq} . SegNet gets the mask of the tumor region from neuroimages that are specific to a given modality. The parameters of the off-the-shelf SegNet are not updated during the training phase, such as nnUnet (Isensee et al., 2020), TransUNet (Chen et al., 2021), and SwinUNet (Cao et al., 2021). The tumor encoder learns how to represent the tumor mask region, particularly texture details and the level of brightness. The quality of the SegNet-reconstructed tumor region is constrained using the loss L_{tumor} . **First stage output:** The private tumor encoder, the private complex encoder and the shared structure encoder for both modalities. **Second stage input:** The input are the query modality neuroimage and the modality-specific tumor encoder, complex encoder and the shared structure encoder from the first stage. The two main components of K-CROSS are $\eta_{complex}$ and η_{nature} . The complex score network yields $\eta_{complex}$, whereas the natural score network yields η_{nature} . The output of the tumor encoder and the structure encoder are combined as the input of the natural score network. The average score for $\eta_{complex}$ and η_{nature} is η_{total} . For η_{total} , K-CROSS uses a straightforward regression model during the training phase, with labels taken from the NIRPS dataset. **Inference:** The input are the query modality neuroimage and the modality-specific tumor encoder, complex encoder and the shared structure encoder from the first stage. The output score is η_{total} .

discrete Fourier transform:

$$F(u, v) = \sum_{x=0}^{M-1} \sum_{y=0}^{N-1} f(x, y) e^{-i2\pi(\frac{ux}{M} + \frac{vy}{N})}, \quad (1)$$

where the MR image size is $M \times N$, (x, y) is the MRI's pixel coordinate, (u, v) is its spatial coordinate in k-space, $F(u, v)$ is its complex frequency value, and e and i stand for the Euler's number and the imaginary unit, respectively. We concentrate on the real and imaginary components of $F(u, v)$. According to (1), we rewrite $F(u, v)$ as follows:

$$F(u, v) = R(u, v) + I(u, v)i = a + bi, \quad (2)$$

where the imaginary and real parts of $F(u, v)$ are $I(u, v)$ and $R(u, v) = a$, respectively. Furthermore, we introduce two key k-space concepts. Here, the amplitude can be defined as:

$$|F(u, v)| = \sqrt{R(u, v)^2 + I(u, v)^2} = \sqrt{a^2 + b^2}. \quad (3)$$

K-CROSS

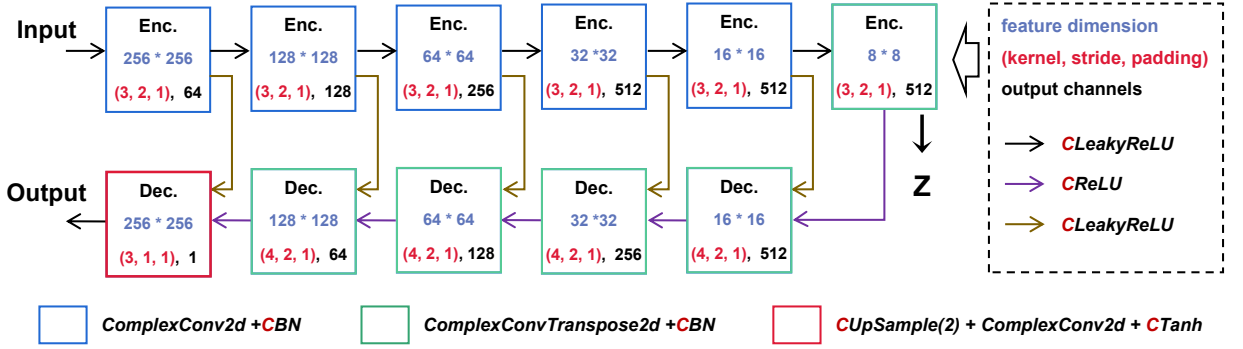


Figure 3: The architecture of complex encoder and decoder. The encoder consists of Complex Conv2d in Section 3.1.2 and Complex BatchNorm in Section 3.1.6. The decoder contains ComplexConvTranspose2d and Complex BatchNorm. The ComplexConvTranspose2d is similar to ComplexConv2d except for the convolution operator. The middle part includes Complex Upsample in Section 3.1.7, Complex Tanh in Section 3.1.5 and Complex Conv2d.

The amplitude is a measure of how strongly a 2D wave reacts to an MR image. We typically visualize k-space using the amplitude.

$$\angle F(u, v) = \arctan \left(\frac{I(u, v)}{R(u, v)} \right) = \arctan \left(\frac{b}{a} \right). \quad (4)$$

The peak shift distance between two 2D sinusoidal waves of the same frequency is referred to as a phase. The phase is the second concept, which is defined in (4).

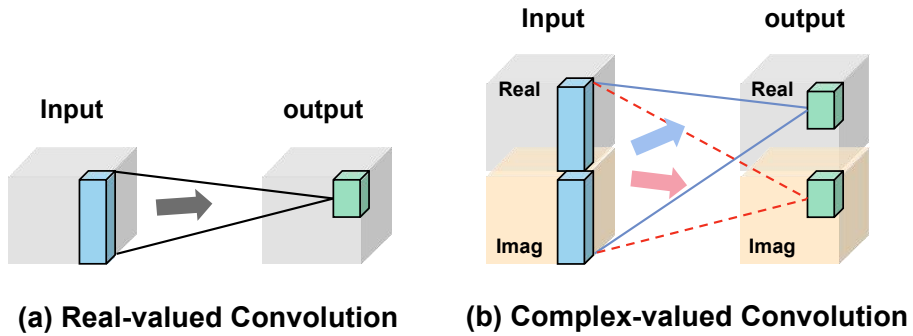


Figure 4: Illustration of complex convolution.

3.1.2. Complex Convolution

The complex-valued convolution (Trabelsi, Bilaniuk, Serdyuk, Subramanian, Santos, Mehri, Rostamzadeh, Bengio and Pal, 2018) is different from the real-valued convolution. Given a complex-valued convolution filter $\mathbf{W} = \mathbf{A} + i\mathbf{B}$ with real-valued matrices \mathbf{A} and \mathbf{B} . The operation is expressed as follows:

$$\mathbf{W} * \mathbf{h} = (\mathbf{A} * \mathbf{x} - \mathbf{B} * \mathbf{y}) + i(\mathbf{B} * \mathbf{x} + \mathbf{A} * \mathbf{y}). \quad (5)$$

The visualization can be found in Fig. 4.

3.1.3. Complex Leaky RELU

It applies separate Leaky RELUs (Maas, 2013) on both the real part $\mathbf{R}(z)$ and the imaginary part $\mathbf{Im}(z)$ of a complex-valued, which is defined as:

$$\mathbb{C}LeakyRELU = LRELU(\mathbf{R}(z)) + i * LRELU(\mathbf{Im}(z)), \quad (6)$$

3.1.4. Complex RELU

It applies separate RELUs (Agarap, 2018) on both the real part $\mathbf{R}(z)$ and the imaginary part $\mathbf{Im}(z)$ of a complex-valued, which is defined as:

$$\mathbb{C}RELU = RELU(\mathbf{R}(z)) + i * RELU(\mathbf{Im}(z)). \quad (7)$$

The visualization is given in Fig. 5.

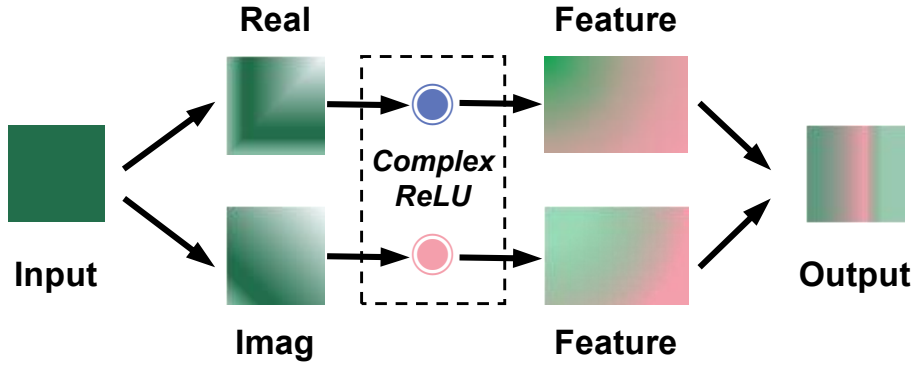


Figure 5: Illustration of complex operator.

3.1.5. Complex Tanh

Complex Tanh applies separate tanh activation (Kalman and Kwasny, 1992) on both the real part $\mathbf{R}(z)$ and imaginary part $\mathbf{Im}(z)$ of a complex-valued, which is defined as:

$$\mathbb{C}Tanh = Tanh(\mathbf{R}(z)) + i * Tanh(\mathbf{Im}(z)). \quad (8)$$

3.1.6. Complex BatchNorm

As described in Cogswell *et al.* (Cogswell, Ahmed, Girshick, Zitnick and Batra, 2016), complex-valued batch normalization could be separately applied into the imaginary part and real part, which could reduce the risk of overfitting. The detail operation is defined as:

$$\mathbb{C}BN = BN(\mathbf{R}(z)) + i * BN(\mathbf{Im}(z)). \quad (9)$$

3.1.7. Complex Upsample

complex-valued upsample algorithm is able to be separately applied to the real part and imaginary part, which is defined as:

$$\mathbb{C}Upsample = Upsample(\mathbf{R}(z)) + i * Upsample(\mathbf{Im}(z)). \quad (10)$$

3.2. Architecture

The two stages of training for K-CROSS are depicted in Fig 2. Encoder-decoder architecture is primarily used in the first stage of K-CROSS to train the tumor encoder, complex encoder, and structure encoder. The complex score network and natural score network are optimized by K-CROSS using a regressor in the second stage. For stage one, the source modality neuroimage and the target modality neuroimage are fed into tumor branch, complex branch and structure branch. A shared cross-modality segmentation network and a personal tumor encoder-decoder make up the

tumor branch. The segmentation network is used to obtain the predicted lesion region. The tumor encoder then captures the brightness and texture features of the lesion region. As for complex branch, the input is converted into k-space by Fourier transform. The function of the private complex encoder is to identify the k-space feature shift. The source modality and the target modality share the structure branches in K-CROSS. The structure's goal is to gather information about the shared structure from both inputs. The architecture and weights of the tumor encoder, complex encoder, and structure encoder are cloned from the first stage in the second stage. The complex score network and the natural score network are optimized by K-CROSS using a regressor.

3.2.1. Complex Branch

A more refined U-Net architecture implemented in k-space makes up the proposed complex encoder. Specifically, each downsampling block in the encoding stage includes complex convolution $\mathbb{C}BN$ and $\mathbb{C}LeakyRELU$. The complex convolution is replaced with the complex transposed convolution for up-sampling during the decoding phase. There is a complex transposed convolution, $\mathbb{C}BN$, and $\mathbb{C}RELU$ in each upsampling block. We apply $\mathbb{C}Upsample$, complex convolution and $\mathbb{C}Tanh$ to reconstruct the images in the final layer of the decoding stage. Fig. 3 shows the complex branch architecture in detail.

3.2.2. Tumor and Structure Branch

As a cross-modality segmentation neural network, the well-trained nnU-Net (Isensee et al., 2020) is used in K-CROSS, with the weights being adjusted in the second stage of training. The modality-specific tumor encoder and decoder are private because the tumor information (the texture details and brightness) from the source modality and the target modality differ. With the exception of the operators using the normal convolution, batch norm, and Leaky RELU, the architecture details of the tumor encoder-decoder and the structure encoder-decoder are similar to those of Fig. 3.

3.2.3. Score Network and Quality Prediction Regressor

We construct a two-layer MLP for quality prediction, considering that the regressor simply maps the output vectors of the triple-path decoder to labeled quality scores. The network is made up of two fully connected layers with 512-256 and 256-1 channels. The complex score network is composed of two complex fully interconnected layers. Its structure is similar to that shown in Fig. 5. However, the operator of the complex score network substitutes MLP layers for $\mathbb{C}RELU$. The natural score network has two fully connected layers as well. The channels of the complex score network and the natural score network are 512-256 and 256-1, respectively. The regressor is trained by using the L_1 loss function.

3.3. Loss Function

3.3.1. Frequency Loss

Directly measuring the distance between two complex vectors is very difficult. Alternatively, recent works are more concerned with the image amplitude. We discover that without the phase information from Fig. 6, which is impossible to reconstruct the entire neuroimage.

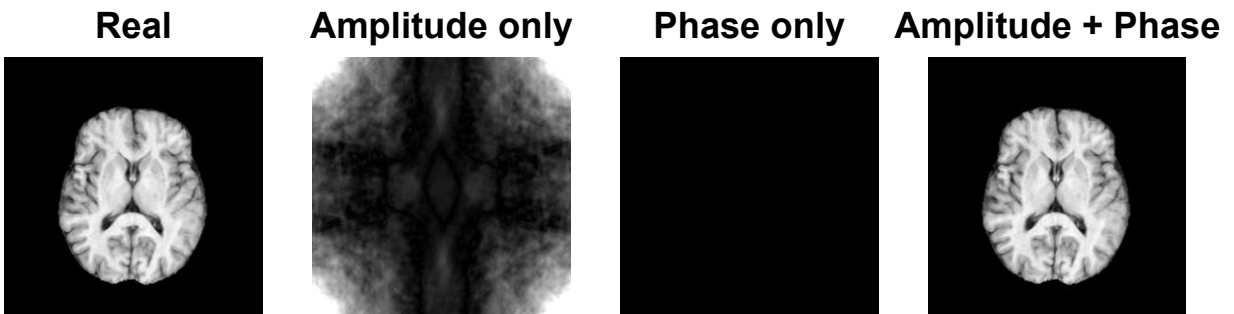


Figure 6: Illustration of the k-space amplitude and phase of images. When only the amplitude or phase is given, the reconstructed image will lose the information of the real image.

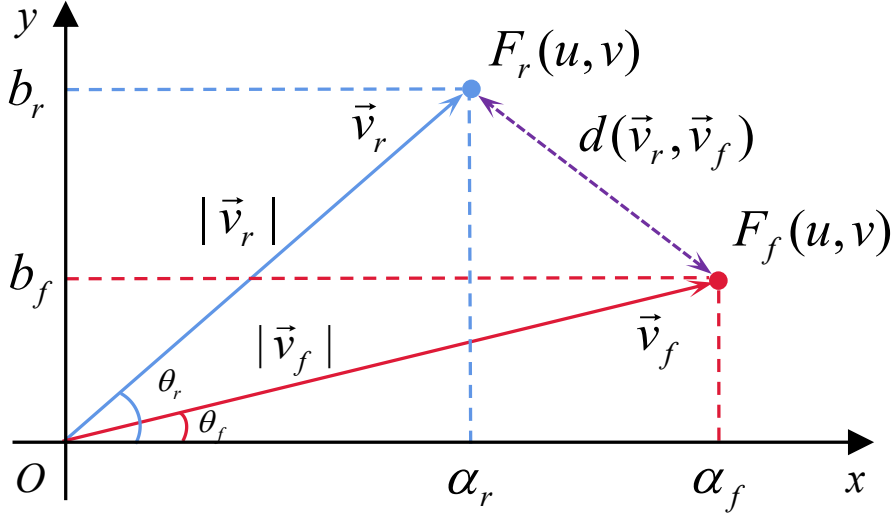


Figure 7: Frequency loss: the distance between \vec{v}_r and \vec{v}_f corresponds to the distance between F_r and F_f .

Our solution is based on the focal frequency loss (Jiang, Dai, Wu and Loy, 2021), as shown in Fig. 7. The hidden k-space of real MRI is $F_r(u, v) = a_r + b_r i$, and the corresponding k-space of synthesis MRI is $F_f(u, v) = a_f + b_f i$. To calculate their distance, we map F_r and F_f into the Euclidean space as \vec{v}_r and \vec{v}_f . Specifically, the lengths of \vec{v}_r and \vec{v}_f are the amplitudes of F_r and F_f , respectively. And the angles θ_r and θ_f correspond to the phases of F_r and F_f , respectively. As a result, the distance between F_r and F_f can be converted to the distance between \vec{v}_r and \vec{v}_f (termed as $d(\vec{v}_r, \vec{v}_f)$), which is defined as follows:

$$d(F_r, F_f) = d(\vec{v}_r, \vec{v}_f) = \|\vec{v}_r - \vec{v}_f\|^2. \quad (11)$$

The complex feature maps are extracted from each layer l of the encoder in the complex U-Net. Each pixel of the complex feature maps for each layer is denoted as $m^l \in \mathbb{R}^{H_l \times W_l \times C_l}$. Finally, we compute spatial and channel averages. As a result, the frequency loss for a complex U-Net is defined as follows:

$$\mathcal{L}_{freq}(m_r^l, m_f^l) = \sum_l \frac{1}{H_l W_l} \sum_{h,w} \|\vec{v}_r - \vec{v}_f\|^2. \quad (12)$$

3.3.2. Similarity Loss

For the similarity loss \mathcal{L}_{simi} , K-CROSS uses the maximum mean discrepancy (MMD) loss (Simonyan and Zisserman, 2015) to measure it. That is, K-CROSS computes the squared population MMD between shared structure encoding of the source modality h_c^s and the target modality h_c^t using a biased statistic. We express this as:

$$\begin{aligned} \mathcal{L}_{simi} = & \frac{1}{(N^s)^2} \sum_{i,j=0}^{N^s} \kappa(h_{c_i}^s, h_{c_j}^s) - \frac{2}{N^s N^t} \sum_{i,j=0}^{N^s, N^t} \kappa(h_{c_i}^s, h_{c_j}^t) \\ & + \frac{1}{(N^t)^2} \sum_{i,j=0}^{N^t} \kappa(h_{c_i}^t, h_{c_j}^t), \end{aligned} \quad (13)$$

where κ is a linear combination of multiple RBF kernels: $\kappa(x_i, x_j) = \sum_n \eta_n \exp \left\{ -\frac{1}{2\sigma_n^2} \|x_i - x_j\|^2 \right\}$, where σ_n is the standard deviation and η_n is the weight for n -th RBF kernel. The similarity loss function encourages the shared structure encoder to learn the invariant structure feature irrespective of the modality.

3.3.3. Tumor Loss

The tumor loss function consists of a Laplacian loss function \mathcal{L}_{lap} and the LPIPS loss function \mathcal{L}_{lips} (Zhang et al., 2018). The Laplacian loss function is defined as :

$$\mathcal{L}_{lap} = \mathbb{E} \|L(x) - L(\hat{x})\|_2^2. \quad (14)$$

The LPIPS loss function is defined as:

$$\mathcal{L}_{lips} = \sum_k \tau^k(\phi^k(x) - \phi^k(\hat{x})). \quad (15)$$

So the tumor loss is described below:

$$\mathcal{L}_{tumor} = \lambda_{lap}\mathcal{L}_{lap} + \lambda_{lips}\mathcal{L}_{lips}. \quad (16)$$

In (15), $\phi(\cdot)$ represents the feature extractor and $\tau(\cdot)$ computes the feature score from the k-th layer of the backbone architecture. As a result, the LPIPS value is the average score of all backbone layers. To compute the LPIPS loss, we used a well-trained VGG (Simonyan and Zisserman, 2015) network. The Laplacian loss is used to identify the tumor region's high-frequency component. Due to LPIPS loss, the real tumor region and the reconstructed tumor region are more similar, which is more consistent with the radiologist's judgment.

3.3.4. Structure Loss

We employ L_1 loss function to extract meaningful semantic structure features, where the structure loss function is defined as:

$$\mathcal{L}_{stru} = \|x - \hat{x}\|_1. \quad (17)$$

3.3.5. Inconsistency Loss

We adopt the MSE loss function to optimize the weights of complex score network n_c and natural score network n_{nat} , where the inconsistency loss is defined as:

$$\mathcal{L}_{inc} = \|\eta_{total} - \eta_{ra}\|_1, \quad (18)$$

where the score of K-CROSS η_{total} is aligned with the scale of the radiologist's rating score η_{ra} via our proposed ranking algorithm. The details of the ranking algorithm can be found in Algorithm 4.

3.3.6. Total Loss

For the first stage, the loss function is described below:

$$\mathcal{L}_{first} = \lambda_1\mathcal{L}_{tumor} + \lambda_2\mathcal{L}_{stru} + \lambda_3\mathcal{L}_{freq} + \lambda_4\mathcal{L}_{sim}. \quad (19)$$

In the second stage, we optimize the parameters of the complex score network and the natural score network via

$$\mathcal{L}_{second} = \mathcal{L}_{inc}. \quad (20)$$

In this work, all weights of λ are set to 1.

3.4. Algorithms

The two stages of training K-CROSS are depicted in Fig 2. The details of two-stage training algorithms and the inference algorithm are described in Algorithm 1, Algorithm 2 and Algorithm 3, respectively. For clarity, Table 1 provides notation descriptions that occurred in our algorithms.

4. NIRPS Dataset and Radiologist Score

To comprehensively evaluate the synthesis performance, we construct a large-scale multi-modal neuroimaging perceptual similarity (NIRPS) dataset with 6,000 radiologist judgments. NIRPS dataset is composed of three subsets generated by CycleGAN (Zhu, Park, Isola and Efros, 2017), MUNIT Huang, Liu, Belongie and Kautz (2018) and

Table 1

Description for notations used in our algorithms.

Notation	Description
s	Source neuroimage
t	Paired target neuroimage
\hat{t}	Synthesized target modality neuroimage
Ω_{ref}	Reference images
Ω_{syn}	Synthesised images
φ_E	Tumor encoder
φ_D	Source tumor decoder
ψ_E	Source complex encoder
ψ_D	Complex decoder
ξ_E	Shared structure encoder
ξ_D	Shared structure decoder
v	Segmentation network
FT	Fourier transform
l	Lesion mask
ζ	K-space function
z	Structural feature
θ_X^n	The parameters of X trained in stage n
n_c	Complex score network
n_{nat}	Natural score network
η_{ra}	Radiologist rating score
η_{total}	K-CROSS score

Algorithm 1: K-CROSS training stage 1

Input : Source neuroimage s , paired target neuroimage t , tumor encoder φ_E , source tumor decoder φ_D , source complex encoder ψ_E , complex decoder ψ_D , shared structure encoder ξ_E , shared structure decoder ξ_D , segmentation network v , Fourier transform FT , lesion mask l , k-space ζ , structural feature z .

Output: The parameters of tumor encoder $\theta_{\varphi_E}^1$, tumor decoder $\theta_{\varphi_D}^1$, complex encoder $\theta_{\psi_E}^1$, complex decoder $\theta_{\psi_D}^1$, structure encoder $\theta_{\xi_E}^1$ and structure decoder $\theta_{\xi_D}^1$.

```

1  $l_t \leftarrow v(t)$  // generate lesion mask of target neuroimage
2  $\zeta_t \leftarrow FT(t)$  // convert k-space of target neuroimage
3  $z_s \leftarrow \xi_E(s)$  // compute structure feature of source neuroimage
4  $z_t \leftarrow \xi_E(t)$  // convert structure feature of target neuroimage
5 while not converged do
6   Update  $\theta_{\varphi_E}^1$  and  $\theta_{\varphi_D}^1$  with  $\kappa_t, \mathcal{L}_{freq}$  in (12)
7   Update  $\theta_{\psi_E}^1$  and  $\theta_{\psi_D}^1$  with  $l_t, \mathcal{L}_{tumor}$  in (16)
8   Update  $\theta_{\xi_E}^1$  and  $\theta_{\xi_D}^1$  with  $z_s, z_t, \mathcal{L}_{simi}$  in (13) and  $\mathcal{L}_{stru}$  in (17)
9 end while

```

UNIT Liu, Breuel and Kautz (2017a). Each set contains 800 images generated by IXI and 1,200 images generated by BraTS. The IXI dataset includes two modalities, PD and T2, while the BraTS dataset includes three modalities, T1, T2, and FLAIR. In both the IXI and BraTS datasets, we randomly select 10 slices for training and collect the training results after each epoch of the model trained over 40 epochs.

IXI (Aljabar, Wolz, Srinivasan, Counsell, Rutherford, Edwards, Hajnal and Rueckert, 2011) collects nearly 600 MR images from normal and healthy subjects in three hospitals. The MR image acquisition protocol for each subject includes T1, T2, PD-weighted images (PD), MRA images, and Diffusion-weighted images. In this paper, we only use T1 (581 cases), T2 (578 cases) and PD (578 cases) data to conduct our experiments, and select the paired data with the

Algorithm 2: K-CROSS training stage 2

Input : Synthesis target modality neuroimage \hat{t} , tumor encoder and its parameters from stage 1: φ_E and $\theta_{\varphi_E}^1$, complex encoder and its parameters from stage 1: ψ_E and $\theta_{\psi_E}^1$, structure encoder and its parameters from stage 1: ξ_E and $\theta_{\xi_E}^1$, complex score network n_c , natural score network n_{nat} .

Output: The parameters of tumor encoder $\theta_{\varphi_E}^2$, complex encoder $\theta_{\psi_E}^2$, structure encoder $\theta_{\xi_E}^2$, complex score network θ_{n_c} , natural score network $\theta_{n_{nat}}$

- 1 $\zeta_{\hat{t}} \leftarrow FT(\hat{t})$ // convert k-space of synthesis target neuroimage
- 2 $l_{\hat{t}} \leftarrow v(\hat{t})$ // generate lesion mask of synthesis target neuroimage
- 3 $f_{complex} \leftarrow \psi_E(\zeta_{\hat{t}})$ // compute the complex feature
- 4 $f_{tumor} \leftarrow \varphi_E(l_{\hat{t}})$ // compute the tumor feature
- 5 $f_{stru} \leftarrow \xi_E(\hat{t})$ // compute the structure feature
- 6 $\eta_{complex} \leftarrow n_c(f_{complex})$ // compute the complex score
- 7 $\eta_{nat} \leftarrow n_{nat}(f_{tumor} + f_{stru})$ // compute the nature score
- 8 $\eta_{total} \leftarrow \eta_{nat} + \eta_{complex}$
- 9 Ranking all η_{total} and get in line with η_{ra}
- 10 **while not converged do**
- 11 | Update θ_{n_c} and $\theta_{n_{nat}}$ with η_{total} , η_{ra} and \mathcal{L}_{inc} in (18)
- 12 **end while**

Algorithm 3: K-CROSS inference

Input : Synthesis target modality neuroimage \hat{t} , tumor encoder and its parameters from stage 1: φ_E and $\theta_{\varphi_E}^1$, complex encoder and its parameters from stage 1: ψ_E and $\theta_{\psi_E}^1$, structure encoder and its parameters from stage 1: ξ_E and $\theta_{\xi_E}^1$, complex score network and its parameters from stage 2: n_c and θ_{n_c} , natural score network and its parameters from stage 2: n_{nat} and $\theta_{n_{nat}}$, Fourier transform FT , segmentation network v .

Output: K-CROSS score η_{total} .

- 1 $\zeta_{\hat{t}} \leftarrow FT(\hat{t})$ // convert k-space of synthesis target neuroimage
- 2 $l_{\hat{t}} \leftarrow v(\hat{t})$ // generate lesion mask of synthesis target neuroimage
- 3 $f_{complex} \leftarrow \psi_E(\zeta_{\hat{t}})$ // compute the complex feature
- 4 $f_{stru} \leftarrow \xi_E(\hat{t})$ // compute the structure feature
- 5 $\eta_{complex} \leftarrow n_c(f_{complex})$ // compute the complex score
- 6 **if** $\hat{t} \in \text{healthy person}$ **then**
- 7 | $\eta_{nat} \leftarrow f_{stru}$
- 8 **else**
- 9 | $l_{\hat{t}} \leftarrow v(\hat{t})$ // generate lesion mask of synthesis target neuroimage
- 10 | $f_{tumor} \leftarrow \varphi_E(l_{\hat{t}})$ // compute the tumor feature
- 11 | $\eta_{nat} \leftarrow n_{nat}(f_{tumor} + f_{stru})$
- 12 **end if**
- 13 $\eta_{total} \leftarrow \eta_{nat} + \eta_{complex}$
- 14 Ranking all η_{total} and get in line with η_{ra}

same ID from the three modes. The image has a non-uniform length on the z-axis with the size of 256 on the x-axis and y-axis. The IXI dataset is not divided into a training set and a test set. Therefore, we randomly split the whole data as the training set (80%) and the test set (20%).

BraTS2021 (Siegel, Miller and Jemal, 2019; Bakas, Kuijf, Menze and Reyes, 2017) is designed for the analysis and diagnosis of brain diseases. The dataset of multi-institutional and pre-operative MRI sequences is made publicly available and includes both training data (1251 cases) and validation data (219 cases). Each 3D volume is 155×240×240 in size and is imaged by four sequences: T1, T2, T1ce, and FLAIR.

Training Data Processing To ensure the validity and diversity of the data, we remove their skulls for each slice, by splitting the three-dimensional volume and choosing slices ranging from 50 to 80 on the z-axis. All images are cropped to 256 pixels in size. During the training stage, we choose a total of 10k images from the IXI and BraTS2021 datasets.

Algorithm 4: Calculate inconsistency by ranking

```

1 Input: reference images  $\Omega_{ref}$ , synthesised images  $\Omega_{syn}$ 
2 Initialize: start = 0, pairwise  $\leftarrow \phi$ , uniform_result  $\leftarrow \phi$ 
3 // count elements in levels
4 recounted = Collection.Counter( $\Omega_{ref}$ )
5 // obtain the sorted level of reference images
6 level = sorted(recounted)
7 // obtain the indices of synthesised images
8 index = numpy.argsort( $\Omega_{syn}$ )
9 // obtain the number of images  $\Omega_{ref}$  in each level
10 for  $l$  in level do
11     end = start + recounted[ $l$ ]
12     pairwise.append([start, end])
13     start = end
14 end for
15 // obtain uniformed results  $\Omega_{syn}$ 
16 for  $v$  in index do
17     for  $i, p$  in enumerate(pairwise) do
18         if  $v$  in range( $p[0], p[1]$ ) then
19             uniform_result.append( $i / \text{len}(\text{level})$ )
20             break
21         end if
22     end for
23 end for
24 // calculate consistency
25 Return:  $\|\Omega_{ref} - \Omega_{syn}\|_1.\text{mean}()$ 

```

4.0.1. Radiologist Score

The NIRPS dataset contains radiologist scores (RS) resulting from manual annotation for each image. It is worth noting that the radiologist score RS includes 10 levels, i.e., $RS \in [0, 0.1, 0.2, \dots, 0.9]$. The higher RS value indicates better-synthesized neuroimage quality. Radiologists give scores according to the level of diagnosis and therapy using the synthesized neuroimage. Fig. 8 gives the distribution result of RS . We can see that synthesized performance varies among the three models and the average RS is in the middle.

4.0.2. How Radiologists Assess?

We prepare the real paired modalities neuroimage dataset M in advance. M consists of source modalities M_s and target modalities M_t . We generate the synthesized target modality neuroimages \hat{M}_t via feeding M_s into the generative model, i.e., CycleGAN, MUNIT and UNIT in NIPRS. Then radiologist gives the score for \hat{M}_t according to the comparison with \hat{M}_t . For instance, we have paired ground-truth modality datasets, T1 and T2. As shown in Fig. 9, we synthesized the fake T2 by feeding T1 into the MUNIT model. The radiologists make direct comparisons between fake T2 and real T2 and give their score for the synthesised quality of T2.

4.0.3. How Radiologists Combine Their Evaluations?

We hire 10 radiologists to evaluate the quality of each synthesized neuroimage. We remove the highest score and the lowest score from all radiologists. The final score is then averaged by the rest score from 8 radiologists.

5. Experiment and Ablation Study

5.1. K-CROSS vs Other Metrics

Table 2 illustrates the inconsistency between metrics and human evaluations of several datasets and generative models, with the highest performance shown in red. The calculation method for inconsistency value is given in Algorithm 4. We evaluate K-CROSS on datasets created by CycleGAN, MUNIT, and UNIT. The first column indicates various IQA methods. The second column indicates which datasets were used to train the K-CROSS model, including

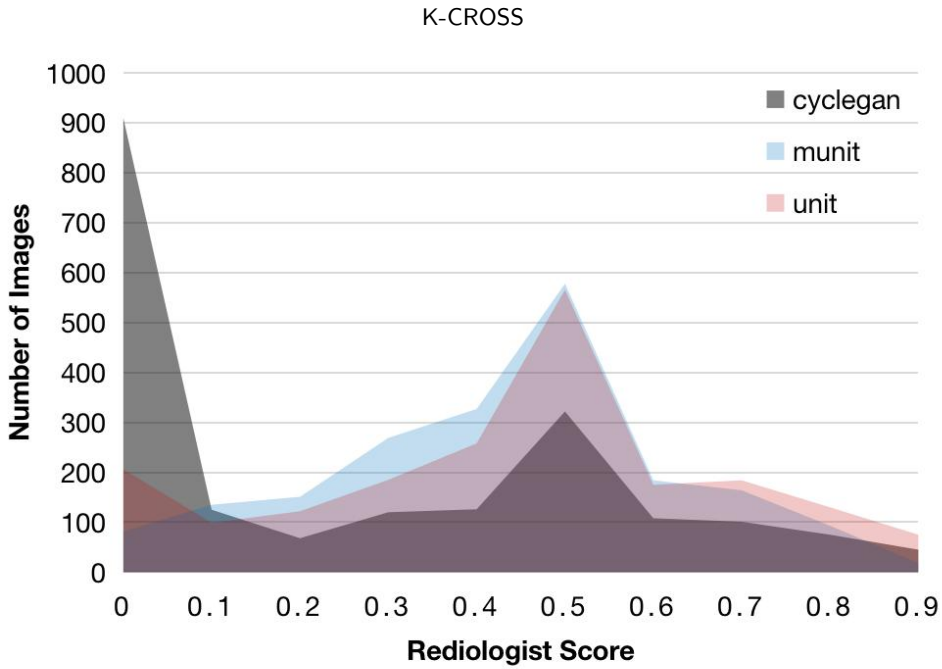


Figure 8: Statistical results of NIRPS.



Figure 9: Labelling tools in our artificial score system. The first column denotes the ground-truth T2 neuroimage. The second column denotes the synthesized T2 neuroimage. The third column is the error map between the ground truth neuroimage and its synthesized one.

IXI or BraTS. From Table 2, our proposed K-CROSS is more compatible with the assessments of radiologists. Note that the IXI dataset is a healthy person dataset. There is no lesion for each neuroimage. So K-CROSS only use the tumor branch and complex branch to assess the quality of neuroimage. The details are described in Section 5.3.

5.2. K-Space Importance

Table 3 records the ablation study of individual branches (the complex branch, tumor branch and structure branch) on various datasets. For example, when we conduct the ablation study of the complex branch, K-CROSS removes the tumor branch and the structure branch in the inference phase. In other words, K-CROSS only obtains $\eta_{complex}$ score. It applies the same setting for the other branches. It can be clearly observed that the complex branch obtains the highest score among the three branches. It strongly indicates the importance of k-space, which reflects the inherent properties of magnetic resonance imaging principles. The second best is the tumor branch. It also verifies the effectiveness of the tumor branch for the lesion disease dataset.

Table 2

Performance comparison of various IQA methods on NIRPS. NIRPS includes three subsets generated by CycleGAN, MUNIT, and UNIT. Specifically, each set consists of 800 images for IXI and 1,200 images for BraTS. Here, IXI and BraTS training sets are used to train our model. The inconsistency is computed, where ↓ is better. The best result is highlighted in red.

Metric	CycleGAN		MUNIT		UNIT	
	IXI	BraTS	IXI	BraTS	IXI	BraTS
Dastaset						
MAE (Chai and Draxler, 2014)	0.3127	0.3335	0.1807	0.2368	0.2462	0.2462
PSNR (Huynh-Thu and Ghanbari, 2008)	0.3387	0.2060	0.1832	0.2515	0.2387	0.2585
SSIM (Wang et al., 2004)	0.3333	0.1998	0.1957	0.2437	0.2523	0.2645
MS-SSIM (Wang et al., 2003)	0.3245	0.1973	0.1934	0.2425	0.2487	0.2521
NLPD (Laparra, Ballé, Berardino and Simoncelli, 2016)	0.3128	0.1961	0.1921	0.2408	0.2466	0.2445
GMSD (Xue, Zhang, Mou and Bovik, 2014)	0.3069	0.1952	0.1910	0.2395	0.2421	0.2432
DeepIQA (Bosse, Maniry, Müller, Wiegand and Samek, 2018)	0.3052	0.1943	0.1827	0.2380	0.2402	0.2410
LPIP (Zhang et al., 2018)	0.3023	0.1921	0.1786	0.2285	0.2398	0.2327
DIST (Ding, Ma, Wang and Simoncelli, 2022)	0.3012	0.1901	0.1725	0.2291	0.2387	0.2230
K-CROSS	0.2878	0.1851	0.1650	0.2246	0.2123	0.2147

Table 3

Effect of k-space importance (complex branch) and tumor branch. The inconsistency is computed, where ↓ is better. The best result is in red and the second best result is in blue.

Model	Structure Branch $\mathcal{L}_{stru} + \mathcal{L}_{simi}$	Complex Branch \mathcal{L}_{freq}	Tumor Branch \mathcal{L}_{tumor}	All
<i>BraTS T1↔FLAIR</i>				
CycleGAN	0.1970	0.1911	0.1920	0.1880
MUNIT	0.2348	0.2273	0.2338	0.2250
UNIT	0.2333	0.2210	0.2248	0.2102
<i>BraTS T2↔FLAIR</i>				
CycleGAN	0.1983	0.1889	0.1953	0.1853
MUNIT	0.2365	0.2272	0.2348	0.2250
UNIT	0.2305	0.2250	0.2297	0.2155
<i>BraTS T1↔T2</i>				
CycleGAN	0.1839	0.1836	0.1953	0.1819
MUNIT	0.2332	0.2258	0.2308	0.2239
UNIT	0.2595	0.2290	0.2298	0.2183

5.3. Metrics for Healthy Person

Table 4 shows K-CROSS performance that surpasses the mainstream IQA methods on the IXI healthy-person dataset. As for assessing the synthesised neuroimage of healthy persons, K-CROSS removes the tumor branch in the inference phase. Because there are no lesions on healthy person datasets. It means that K-CROSS only combines $\eta_{complex}$ and the score of the structure encoder as the final score. From Table 4, it can be obviously observed that K-CROSS complex branch score $\eta_{complex}$ (blue value) has surpassed the other IQA methods, which identify the importance of k-space for MRI of healthy persons. Thus, K-CROSS still be able to serve as the metric for the synthesized quality of healthy person’s neuroimage.

Table 4

Metric performance for healthy persons on IXI. The inconsistency is computed, where \downarrow is better. The best result is in red and the second best result is in blue.

Metric	CycleGAN	MUNIT	UNIT
MAE (Chai and Draxler, 2014)	0.3160	0.1809	0.2442
PSNR (Huynh-Thu and Ghanbari, 2008)	0.3388	0.1835	0.2419
SSIM (Wang et al., 2004)	0.3352	0.1962	0.2423
MS-SSIM (Wang et al., 2003)	0.3238	0.1945	0.2418
NLPD (Laparra et al., 2016)	0.3135	0.1918	0.2409
GMSD (Xue et al., 2014)	0.3090	0.1908	0.2398
DeepIQA (Bosse et al., 2018)	0.3043	0.1856	0.2381
LPIP (Zhang et al., 2018)	0.3022	0.1810	0.2374
DIST (Ding et al., 2022)	0.3056	0.1805	0.2356
K-CROSS (\mathcal{L}_{stru})	0.3078	0.1790	0.2318
K-CROSS(\mathcal{L}_{comp})	0.3045	0.1618	0.2233
K-CROSS ($\mathcal{L}_{stru} + \mathcal{L}_{comp}$)	0.2876	0.1610	0.2150

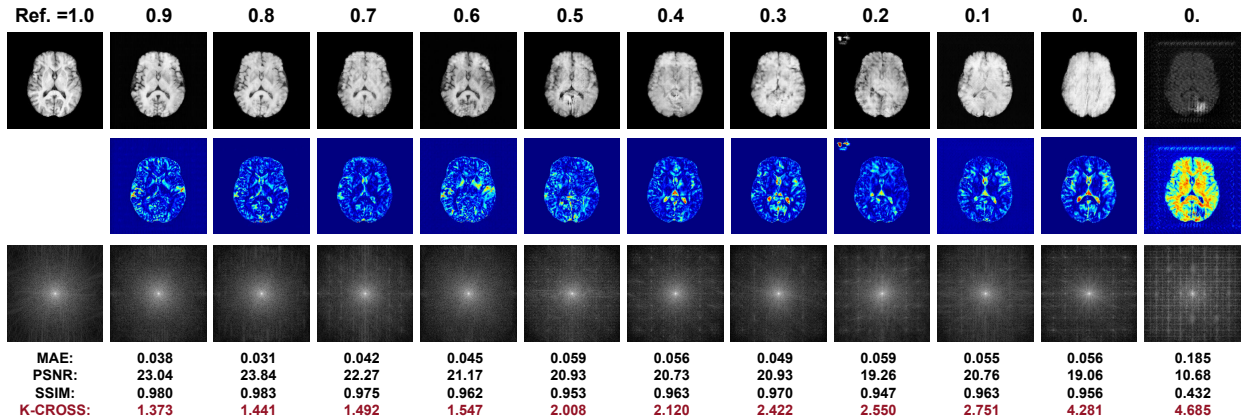


Figure 10: Visualization of the NIRPS dataset. The number above each synthesized neuroimage is the radiologist's score. The blue map denotes the error map between the synthesis neuroimage data and the reference image. The third row represents the k-space map. A higher value of MAE, PSNR, SSIM and radiologist' score indicates higher performance of the synthesis quality. A lower value of K-CROSS indicates a higher performance of the synthesis quality. It's easily observed that K-CROSS is consistent with the order of the radiologist's score when the synthesis quality deteriorates but PSNR, SSIM and MAE are not.

5.4. Segmentation Network Effect

Table 5 shows K-CROSS remains stable performance even using different state-of-the-art medical segmentation models. Note that the parameters of the pre-trained segmentation network are frozen during the training phase. The first column denotes the segmentation method. We calculate the variance score of the K-CROSS value for CycleGAN, MUNIT and UNIT by using different segmentation backbone models. We find that the variance of K-CROSS performance is tiny (0.2%, 0.3%, and 0.2%). Hence, the performance of K-CROSS is not affected by the segmentation model.

Table 5

The effect of segmentation network for K-CROSS value for various generative models of NIRPS.

Segmentation Model	CycleGAN	MUNIT	UNIT
nnUnet (Isensee et al., 2020)	0.1872	0.2246	0.2160
AttnUnet (Schlemper, Oktay, Schaap, Heinrich, Kainz, Glocker and Rueckert, 2019)	0.1873	0.2268	0.2157
SETR (Zheng, Lu, Zhao, Zhu, Luo, Wang, Fu, Feng, Xiang, Torr and Zhang, 2021)	0.1852	0.2254	0.2162
CoTr (Xie, Zhang, Shen and Xia, 2021)	0.1856	0.2244	0.2154
TransUNet (Chen et al., 2021)	0.1862	0.2247	0.2162
SwinUNet (Cao et al., 2021)	0.1845	0.2252	0.2158

Table 6

K-CROSS on NIRPS (CycleGAN). The inconsistency is computed, where ↓ is better. The best result is in red and the second best result is in blue.

Training Set (BraTS)	T1-FLAIR	T2-FLAIR	T1-T2
Test Set (IXI)	PD-T2	PD-T2	PD-T2
MAE (Chai and Draxler, 2014)	0.3208	0.3321	0.3228
PSNR (Huynh-Thu and Ghanbari, 2008)	0.3190	0.3270	0.3261
SSIM (Wang et al., 2004)	0.3231	0.3231	0.3212
MS-SSIM (Wang et al., 2003)	0.3189	0.3180	0.3128
NLPD (Laparra et al., 2016)	0.3176	0.3163	0.3090
GMSD (Xue et al., 2014)	0.3067	0.3154	0.3067
DeepIQA (Bosse et al., 2018)	0.3058	0.3124	0.3045
LPIP (Zhang et al., 2018)	0.3033	0.3056	0.3039
DIST (Ding et al., 2022)	0.3021	0.3032	0.3006
K-CROSS (\mathcal{L}_{stru})	0.3018	0.3013	0.2990
K-CROSS (\mathcal{L}_{freq})	0.3015	0.2997	0.2953
K-CROSS ($\mathcal{L}_{stru} + \mathcal{L}_{freq}$)	0.2893	0.2950	0.2890

5.5. General Metric? Overcoming Domain Gap

The purpose of this paper is to demonstrate that K-CROSS is capable of serving as the standard measure for MRI datasets. We conduct extensive experiments and the results are given in Table 6, Table 7, and Table 8 to demonstrate that K-CROSS is not affected by dataset domain gap and the generative model. The training dataset is the BraTS dataset, and the test dataset is IXI. As described in Section 5.3, we remove the tumor branch score, when K-CROSS evaluates the quality of neuroimage in healthy cases. We also observe that K-CROSS averagely surpasses DIST and LPIP (SOTA for natural image) by 7.8% and 16.5%, respectively, which proves that K-CROSS is built upon the basis of MRI principle instead of only on the natural image level. From this ablation study, we demonstrate that the performance of K-CROSS ($\mathcal{L}_{stru} + \mathcal{L}_{freq}$) is stable across several MRI datasets, with the potential to serve as a generic measure for evaluating the quality of the synthesized MRI.

6. Conclusion

In this paper, we proposed a new metric K-CROSS to evaluate the performance of medical images synthesized, which is based on the principle of magnetic resonance imaging. To improve the reconstruction capability during

Table 7

K-CROSS on the NIRPS dataset (MUNIT). The inconsistency is computed, where ↓ is better. The best result is in red and the second best result is in blue.

Training Set Test Set	BraTS (T1-FLAIR) IXI (PD-T2)	BraTS (T2-FLAIR) IXI (PD-T2)	BraTS(T1-T2) IXI (PD-T2)
MAE (Chai and Draxler, 2014)	0.1872	0.1865	0.1842
PSNR (Huynh-Thu and Ghanbari, 2008)	0.1853	0.1873	0.1853
SSIM (Wang et al., 2004)	0.1967	0.1986	0.1982
MS-SSIM (Wang et al., 2003)	0.1932	0.1952	0.1923
NLPD (Laparra et al., 2016)	0.1945	0.1943	0.1921
GMSD (Xue et al., 2014)	0.1920	0.1934	0.1932
DeepIQA (Bosse et al., 2018)	0.1835	0.1845	0.1856
LPIP (Zhang et al., 2018)	0.1783	0.1754	0.1784
DIST (Ding et al., 2022)	0.1742	0.1731	0.1786
K-CROSS (\mathcal{L}_{stru})	0.1713	0.1720	0.1790
K-CROSS (\mathcal{L}_{freq})	0.1703	0.1709	0.1692
K-CROSS ($\mathcal{L}_{stru} + \mathcal{L}_{freq}$)	0.1688	0.1693	0.1617

Table 8

K-CROSS on the NIRPS dataset (UNIT). The inconsistency is computed, where ↓ is better. The best result is in red and the second best result is in blue.

Training Set Test Set	BraTS (T1-FLAIR) IXI (PD-T2)	BraTS (T2-FLAIR) IXI (PD-T2)	BraTS (T1-T2) IXI (PD-T2)
MAE (Chai and Draxler, 2014)	0.2468	0.2445	0.2480
PSNR (Huynh-Thu and Ghanbari, 2008)	0.2421	0.2410	0.2410
SSIM (Wang et al., 2004)	0.2545	0.2505	0.2470
MS-SSIM (Wang et al., 2003)	0.2486	0.2474	0.2463
NLPD (Laparra et al., 2016)	0.2481	0.2461	0.2450
GMSD (Xue et al., 2014)	0.2410	0.2388	0.2478
DeepIQA (Bosse et al., 2018)	0.2398	0.2376	0.2391
LPIP (Zhang et al., 2018)	0.2352	0.2341	0.2384
DIST (Ding et al., 2022)	0.2348	0.2337	0.2386
K-CROSS (\mathcal{L}_{stru})	0.2323	0.2320	0.2250
K-CROSS (\mathcal{L}_{freq})	0.2190	0.2195	0.2250
K-CROSS ($\mathcal{L}_{stru} + \mathcal{L}_{freq}$)	0.2188	0.2188	0.2175

K-CROSS training, a complex U-Net was developed. As for training a learning-based full IQA metric, we further constructed a large-scale multi-modal neuroimaging perceptual similarity (NIRPS) dataset. The experimental results indicate that K-CROSS is a useful indicator for evaluating the quality of the medical data generated. However, our method heavily relies on deep learning-based techniques but without directly injecting the knowledge of radiologists into K-CROSS. In the future, K-CROSS should combine causal inference methods to improve interpretability.

Acknowledgment

This work is partially supported by the National Key R&D Program of China (Grant NO. 2022YFF1202903) and the National Natural Science Foundation of China (Grant NO. 62122035, 61972188, and 62206122).

CRedit authorship contribution statement

Guoyang Xie: Conceptualization, Methodology, Data Curation, Validation, Visualization, Writing - original draft & editing. **Jinbao Wang:** Conceptualization, Methodology, Data Curation, Investigation, Writing - original draft & editing. **Yawen Huang:** Conceptualization, Methodology, Investigation, Writing - review & editing, Supervision. **Jiayi Lyu:** Data Curation, Visualization, Writing - review & editing. **Feng Zheng:** Supervision, Project administration, Funding acquisition, Writing - review & editing. **Yefeng Zheng:** Supervision, Writing - review & editing. **Yaochu Jin:** Supervision, Writing - review & editing.

References

- Agarap, A.F., 2018. Deep learning using rectified linear units (relu). ArXiv abs/1803.08375.
- Aljabar, P., Wolz, R., Srinivasan, L., Counsell, S.J., Rutherford, M.A., Edwards, A.D., Hajnal, J.V., Rueckert, D., 2011. A combined manifold learning analysis of shape and appearance to characterize neonatal brain development. *IEEE Transactions on Medical Imaging* 30, 2072–2086.
- Bakas, S., Kuijf, H.J., Menze, B.H., Reyes, M., 2017. Brainlesion: Glioma, multiple sclerosis, stroke and traumatic brain injuries, in: *Lecture Notes in Computer Science*.
- Bosse, S., Maniry, D., Müller, K.R., Wiegand, T., Samek, W., 2018. Deep neural networks for no-reference and full-reference image quality assessment. *IEEE Transactions on Image Processing* 27, 206–219.
- Bosse, S., Maniry, D., Wiegand, T., Samek, W., 2016. A deep neural network for image quality assessment. 2016 IEEE International Conference on Image Processing (ICIP), 3773–3777.
- Cao, H., Wang, Y., Chen, J., Jiang, D., Zhang, X., Tian, Q., Wang, M., 2021. Swin-unet: Unet-like pure transformer for medical image segmentation. ArXiv abs/2105.05537.
- Chai, T., Draxler, R.R., 2014. Root mean square error (rmse) or mean absolute error (mae)? – arguments against avoiding rmse in the literature. *Geoscientific Model Development* 7, 1247–1250.
- Che, T., Li, Y., Jacob, A.P., Bengio, Y., Li, W., 2017. Mode regularized generative adversarial networks. ArXiv abs/1612.02136.
- Chen, C., Dou, Q., Chen, H., Qin, J., Heng, P.A., 2020. Unsupervised bidirectional cross-modality adaptation via deeply synergistic image and feature alignment for medical image segmentation. *IEEE Transactions on Medical Imaging* 39, 2494–2505.
- Chen, J., Lu, Y., Yu, Q., Luo, X., Adeli, E., Wang, Y., Lu, L., Yuille, A.L., Zhou, Y., 2021. Transunet: Transformers make strong encoders for medical image segmentation. ArXiv abs/2102.04306.
- Cogswell, M., Ahmed, F., Girshick, R.B., Zitnick, C.L., Batra, D., 2016. Reducing overfitting in deep networks by decorrelating representations. *CoRR abs/1511.06068*.
- Dar, S.U.H., Yurt, M., Karacan, L., Erdem, A., Erdem, E., Çukur, T., 2019. Image synthesis in multi-contrast mri with conditional generative adversarial networks. *IEEE Transactions on Medical Imaging* 38, 2375–2388.
- Ding, K., Ma, K., Wang, S., Simoncelli, E.P., 2022. Image quality assessment: Unifying structure and texture similarity. *IEEE Transactions on Pattern Analysis and Machine Intelligence* 44, 2567–2581.
- Elad, M., 2012. Sparse and redundant representation modeling—what next? *IEEE Signal Processing Letters* 19, 922–928.
- Gao, S., Tsang, I.W.H., Chia, L.T., 2012. Laplacian sparse coding, hypergraph laplacian sparse coding, and applications. *IEEE Transactions on Pattern Analysis and Machine Intelligence* 35, 92–104.
- Gretton, A., Sriperumbudur, B.K., Sejdinovic, D., Strathmann, H., Balakrishnan, S., Pontil, M., Fukumizu, K., 2012. Optimal kernel choice for large-scale two-sample tests, in: *NIPS*.
- Guo, P., Wang, P., Yasarla, R., Zhou, J., Patel, V.M., Jiang, S., 2021. Anatomic and molecular mr image synthesis using confidence guided cnns. *IEEE Transactions on Medical Imaging* 40, 2832–2844.
- Heusel, M., Ramsauer, H., Unterthiner, T., Nessler, B., Hochreiter, S., 2017. Gans trained by a two time-scale update rule converge to a local nash equilibrium, in: *NIPS*.
- Huang, X., Liu, M.Y., Belongie, S., Kautz, J., 2018. Multimodal unsupervised image-to-image translation, in: *Proceedings of the European conference on computer vision (ECCV)*, pp. 172–189.
- Huang, Y., Zheng, F., Cong, R., Huang, W., Scott, M.R., Shao, L., 2020a. Mcmt-gan: Multi-task coherent modality transferable gan for 3d brain image synthesis. *IEEE Transactions on Image Processing* 29, 8187–8198.
- Huang, Y., Zheng, F., Wang, D., Jiang, J., Wang, X., Shao, L., 2020b. Super-resolution and inpainting with degraded and upgraded generative adversarial networks, in: *IJCAI*.
- Huynh-Thu, Q., Ghanbari, M., 2008. Scope of validity of psnr in image/video quality assessment. *Electronics Letters* 44, 800–801.
- Isensee, F., Jaeger, P.F., Kohl, S.A.A., Petersen, J., Maier-Hein, K., 2020. nnu-net: a self-configuring method for deep learning-based biomedical image segmentation. *Nature methods*.
- Jiang, G., Lu, Y., Wei, J., Xu, Y., 2019. Synthesize mammogram from digital breast tomosynthesis with gradient guided cgans, in: *International Conference on Medical Image Computing and Computer-Assisted Intervention*, Springer. pp. 801–809.
- Jiang, L., Dai, B., Wu, W., Loy, C.C., 2021. Focal frequency loss for image reconstruction and synthesis. 2021 IEEE/CVF International Conference on Computer Vision (ICCV), 13899–13909.

- Jiao, J., Namburete, A.I.L., Papageorghiou, A.T., Noble, J.A., 2020. Self-supervised ultrasound to mri fetal brain image synthesis. *IEEE Transactions on Medical Imaging* 39, 4413–4424.
- Kalman, B., Kwassny, S., 1992. Why tanh: choosing a sigmoidal function, in: [Proceedings 1992] IJCNN International Joint Conference on Neural Networks, pp. 578–581 vol.4. doi:10.1109/IJCNN.1992.227257.
- Kong, L., Lian, C., Huang, D., Li, Z., Hu, Y., Zhou, Q., 2021. Breaking the dilemma of medical image-to-image translation. *arXiv:2110.06465*.
- Laparra, V., Ballé, J., Berardino, A., Simoncelli, E.P., 2016. Perceptual image quality assessment using a normalized laplacian pyramid, in: HVEL.
- Li, H., Wu, P., Wang, Z., Mao, J.F., Alsaadi, F.E., Zeng, N., 2022. A generalized framework of feature learning enhanced convolutional neural network for pathology-image-oriented cancer diagnosis. *Computers in biology and medicine* 151 Pt A, 106265.
- taek Lim, H., Kim, H.G., Ro, Y.M., 2018. Vr iqa net: Deep virtual reality image quality assessment using adversarial learning. 2018 IEEE International Conference on Acoustics, Speech and Signal Processing (ICASSP), 6737–6741.
- Lin, K.Y., Wang, G., 2018. Hallucinated-iqa: No-reference image quality assessment via adversarial learning. 2018 IEEE/CVF Conference on Computer Vision and Pattern Recognition, 732–741.
- Liu, M., Breuel, T.M., Kautz, J., 2017a. Unsupervised image-to-image translation networks, in: NIPS, pp. 700–708.
- Liu, X., van de Weijer, J., Bagdanov, A.D., 2017b. Rankiqa: Learning from rankings for no-reference image quality assessment. 2017 IEEE International Conference on Computer Vision (ICCV), 1040–1049.
- Maas, A.L., 2013. Rectifier nonlinearities improve neural network acoustic models.
- Mittal, A., Soundararajan, R., Bovik, A.C., 2013. Making a “completely blind” image quality analyzer. *IEEE Signal Processing Letters* 20, 209–212.
- Moorthy, A.K., Bovik, A.C., 2011. Blind image quality assessment: From natural scene statistics to perceptual quality. *IEEE Transactions on Image Processing* 20, 3350–3364.
- Ren, H., Chen, D., Wang, Y., 2018. Ran4iqa: Restorative adversarial nets for no-reference image quality assessment, in: AAAI.
- Ren, M., Dey, N., Fishbaugh, J., Gerig, G., 2021. Segmentation-renormalized deep feature modulation for unpaired image harmonization. *IEEE Transactions on Medical Imaging* 40, 1519–1530.
- Rubinstein, R., Bruckstein, A.M., Elad, M., 2010. Dictionaries for sparse representation modeling. *Proceedings of the IEEE* 98, 1045–1057.
- Salimans, T., Goodfellow, I.J., Zaremba, W., Cheung, V., Radford, A., Chen, X., 2016. Improved techniques for training gans, in: NIPS.
- Schlemper, J., Oktay, O., Schaap, M., Heinrich, M.P., Kainz, B., Glocker, B., Rueckert, D., 2019. Attention gated networks: Learning to leverage salient regions in medical images. *Medical image analysis* 53, 197 – 207.
- Sharma, A., Hamarneh, G., 2020. Missing mri pulse sequence synthesis using multi-modal generative adversarial network. *IEEE Transactions on Medical Imaging* 39, 1170–1183.
- Shen, L., Zhu, W., Wang, X., Xing, L., Pauly, J.M., Turkbey, B., Harmon, S.A., Sanford, T., Mehralivand, S., Choyke, P.L., Wood, B.J., Xu, D., 2021. Multi-domain image completion for random missing input data. *IEEE Transactions on Medical Imaging* 40, 1113–1122.
- Siegel, R.L., Miller, K.D., Jemal, A., 2019. *Cancer statistics, 2019*. CA: A Cancer Journal for Clinicians 69.
- Simonyan, K., Zisserman, A., 2015. Very deep convolutional networks for large-scale image recognition. *CoRR abs/1409.1556*.
- Szegedy, C., Vanhoucke, V., Ioffe, S., Shlens, J., Wojna, Z., 2016. Rethinking the inception architecture for computer vision. 2016 IEEE Conference on Computer Vision and Pattern Recognition (CVPR), 2818–2826.
- Talebi, H., Milanfar, P., 2018. Nima: Neural image assessment. *IEEE Transactions on Image Processing* 27, 3998–4011.
- Trabelsi, C., Bilaniuk, O., Serdyuk, D., Subramanian, S., Santos, J.F., Mehri, S., Rostamzadeh, N., Bengio, Y., Pal, C.J., 2018. Deep complex networks. *ArXiv abs/1705.09792*.
- Wang, Y., Zhou, L., Wang, L., Yu, B., Zu, C., Lalush, D.S., Lin, W., Wu, X., Zhou, J., Shen, D., 2018. Locality adaptive multi-modality gans for high-quality pet image synthesis. *Medical image computing and computer-assisted intervention : MICCAI ... International Conference on Medical Image Computing and Computer-Assisted Intervention* 11070, 329–337.
- Wang, Z., Bovik, A.C., Sheikh, H.R., Simoncelli, E.P., 2004. Image quality assessment: from error visibility to structural similarity. *IEEE Transactions on Image Processing* 13, 600–612.
- Wang, Z., Simoncelli, E.P., Bovik, A.C., 2003. Multi-scale structural similarity for image quality assessment.
- Wu, P., Wang, Z., Zheng, B., Li, H., Alsaadi, F.E., Zeng, N., 2023. Aggn: Attention-based glioma grading network with multi-scale feature extraction and multi-modal information fusion. *Computers in biology and medicine* 152, 106457.
- Xie, Y., Zhang, J., Shen, C., Xia, Y., 2021. Cotr: Efficiently bridging cnn and transformer for 3d medical image segmentation, in: MICCAI.
- Xu, Q., Huang, G., Yuan, Y., Guo, C., Sun, Y., Wu, F., Weinberger, K.Q., 2018. An empirical study on evaluation metrics of generative adversarial networks. *ArXiv abs/1806.07755*.
- Xue, W., Zhang, L., Mou, X., Bovik, A.C., 2014. Gradient magnitude similarity deviation: A highly efficient perceptual image quality index. *IEEE Transactions on Image Processing* 23, 684–695.
- Yang, H., Sun, J., Yang, L., Xu, Z., 2021. A unified hyper-gan model for unpaired multi-contrast mr image translation.
- Yu, B., Zhou, L., Wang, L., Frripp, J., Bourgeat, P.T., 2018. 3d cgan based cross-modality mr image synthesis for brain tumor segmentation. 2018 IEEE 15th International Symposium on Biomedical Imaging (ISBI 2018), 626–630.
- Yu, B., Zhou, L., Wang, L., Shi, Y., Frripp, J., Bourgeat, P.T., 2020. Sample-adaptive gans: Linking global and local mappings for cross-modality mr image synthesis. *IEEE Transactions on Medical Imaging* 39, 2339–2350.
- Yu, Z., Zhai, Y., Han, X., Peng, T., Zhang, X.Y., 2021. Mousegan: Gan-based multiple mri modalities synthesis and segmentation for mouse brain structures.
- Zeng, G., Zheng, G., 2019. Hybrid generative adversarial networks for deep mr to ct synthesis using unpaired data.
- Zhang, L., Zhang, L., Mou, X., Zhang, D., 2011. Fsim: A feature similarity index for image quality assessment. *IEEE Transactions on Image Processing* 20, 2378–2386.
- Zhang, R., Isola, P., Efros, A.A., Shechtman, E., Wang, O., 2018. The unreasonable effectiveness of deep features as a perceptual metric. 2018 IEEE/CVF Conference on Computer Vision and Pattern Recognition, 586–595.

- Zhang, W., Ma, K., Zhai, G., Yang, X., 2021. Uncertainty-aware blind image quality assessment in the laboratory and wild. *IEEE Transactions on Image Processing* 30, 3474–3486.
- Zheng, S., Lu, J., Zhao, H., Zhu, X., Luo, Z., Wang, Y., Fu, Y., Feng, J., Xiang, T., Torr, P.H.S., Zhang, L., 2021. Rethinking semantic segmentation from a sequence-to-sequence perspective with transformers. *2021 IEEE/CVF Conference on Computer Vision and Pattern Recognition (CVPR)*, 6877–6886.
- Zhou, B., Liu, C., Duncan, J.S., 2021. Anatomy-constrained contrastive learning for synthetic segmentation without ground-truth, in: *MICCAI*.
- Zhu, J.Y., Park, T., Isola, P., Efros, A.A., 2017. Unpaired image-to-image translation using cycle-consistent adversarial networks, in: *Proceedings of the IEEE international conference on computer vision*, pp. 2223–2232.
- Zuo, Q., Zhang, J., Yang, Y., 2021. Dmc-fusion: Deep multi-cascade fusion with classifier-based feature synthesis for medical multi-modal images. *IEEE Journal of Biomedical and Health Informatics* 25, 3438–3449.



Guoyang Xie received the Bachelor and MPhil Degrees from University of Electronic Science and Technology of China, Hong Kong University of Science and Technology in 2009 and 2013, respectively. He is pursuing the PhD degree from University of Surrey. Prior to that, he was the Principle Perception Algorithm Engineer in Baidu and GAC, respectively. His research interests include anomaly detection, medical imaging, neural architecture search, and federated learning.



Jinbao Wang received his Ph.D. degree from the University of Chinese Academy of Sciences (UCAS) in 2019. He is currently an Assistant Professor at the National Engineering Laboratory for Big Data System Computing, Shenzhen University, Shenzhen, China. His research interests include digital human modeling and driving, image anomaly detection, computer vision, and machine learning.



Yawen Huang received the M.Sc. and Ph.D. degrees from the Department of Electronic and Electrical Engineering, The University of Sheffield, Sheffield, U.K., in 2015 and 2018, respectively. She is currently a Senior Scientist of Tencent Jarvis Laboratory, Shenzhen, China. Her research interests include computer vision, machine learning, medical imaging, deep learning, and practical AI for computer-aided diagnosis.



Lyu Jiayi, born in 1999, graduated in 2021 from Capital Normal University with a bachelor's degree in computer science and technology. She is now pursuing a Ph.D. in computer applications at the School of Engineering Science, Chinese Academy of Sciences.



Feng Zheng (Member, IEEE) received the Ph.D. degree from The University of Sheffield, Sheffield, U.K., in 2017. He is currently an Assistant Professor with the Department of Computer Science and Engineering, Southern University of Science and Technology, Shenzhen, China. His research interests include machine learning, computer vision, and human-computer interaction.



Yefeng Zheng (Fellow, IEEE) received the B.E. and M.E. degrees from Tsinghua University, Beijing, in 1998 and 2001, respectively, and the Ph.D. degree from the University of Maryland, College Park, MD, USA, in 2005. After graduation, he joined Siemens Corporate Research, Princeton, NJ, USA. He is currently the Director and the Distinguished Scientist of Tencent Jarvis Laboratory, Shenzhen, China, leading the company's initiative on Medical AI. His research interests include medical image analysis, graph data mining, and deep learning. Dr. Zheng is a fellow of the American Institute for Medical and Biological Engineering (AIMBE).



Yaochu Jin (Fellow, IEEE) received the B.Sc., M.Sc., and Ph.D. degrees from Zhejiang University, Hangzhou, China, in 1988, 1991, and 1996, respectively, and the Dr.-Ing. degree from Ruhr University Bochum, Germany, in 2001. He is presently Chair Professor of AI, Head of the Trustworthy and General AI Lab, School of Engineering, Westlake University, Hangzhou, China. Prior to that, he was Alexander von Humboldt Professor for Artificial Intelligence endowed by the German Federal Ministry of Education and Research, with the Faculty of Technology, Bielefeld University, Germany from 2021 to 2023, and Surrey Distinguished Chair, Professor in Computational Intelligence, Department of Computer Science, University of Surrey, Guildford, U.K. from 2010 to 2021. He was also "Finland Distinguished Professor" with University of Jyväskylä, Finland, and "Changjiang Distinguished Visiting Professor" with the Northeastern University, China from 2015 to 2017. His main research interests include evolutionary optimization, evolutionary machine learning, trustworthy AI, and evolutionary developmental AI. Prof Jin is the President of the IEEE Computational Intelligence Society and Editor-in-Chief of *Complex & Intelligent Systems*. He was named by the Web of Science as "a Highly Cited Researcher" from 2019 to 2023 consecutively. He is a Member of Academia Europaea.